



Cite this: *Chem. Sci.*, 2023, **14**, 6915

All publication charges for this article have been paid for by the Royal Society of Chemistry

## Scrutinizing formally $\text{Ni}^{\text{IV}}$ centers through the lenses of core spectroscopy, molecular orbital theory, and valence bond theory†

Ida M. DiMucci,<sup>a</sup> Charles J. Titus,<sup>b</sup> Dennis Nordlund,<sup>c</sup> James R. Bour,<sup>‡,d</sup> Eugene Chong,<sup>d</sup> Dylan P. Grigas,<sup>a</sup> Chi-Herng Hu,<sup>e</sup> Mikhail D. Kosobokov,<sup>f</sup> Caleb D. Martin,<sup>g</sup> Liviu M. Mirica,<sup>g</sup> Noel Nebra,<sup>h</sup> David A. Vicic,<sup>g</sup> Lydia L. Yorks,<sup>g</sup> Sam Yruegas,<sup>g</sup> Samantha N. MacMillan,<sup>g</sup> Jason Shearer<sup>g</sup> and Kyle M. Lancaster<sup>g</sup>

Nickel K- and  $\text{L}_{2,3}$ -edge X-ray absorption spectra (XAS) are discussed for 16 complexes and complex ions with nickel centers spanning a range of formal oxidation states from II to IV. K-edge XAS alone is shown to be an ambiguous metric of physical oxidation state for these Ni complexes. Meanwhile,  $\text{L}_{2,3}$ -edge XAS reveals that the physical d-counts of the formally  $\text{Ni}^{\text{IV}}$  compounds measured lie well above the d<sup>6</sup> count implied by the oxidation state formalism. The generality of this phenomenon is explored computationally by scrutinizing 8 additional complexes. The extreme case of  $\text{Ni}_6^{2-}$  is considered using high-level molecular orbital approaches as well as advanced valence bond methods. The emergent electronic structure picture reveals that even highly electronegative F-donors are incapable of supporting a physical d<sup>6</sup>  $\text{Ni}^{\text{IV}}$  center. The reactivity of  $\text{Ni}^{\text{IV}}$  complexes is then discussed, highlighting the dominant role of the ligands in this chemistry over that of the metal centers.

Received 18th April 2023  
Accepted 30th May 2023

DOI: 10.1039/d3sc02001k  
[rsc.li/chemical-science](http://rsc.li/chemical-science)

## Introduction

Motivated in part by the desire to replace effective but costly Pd catalysts with more earth-abundant, first-row transition metal surrogates, chemists have explored the synthesis and reactivity

of organometallic Ni complexes for use in C–H activation<sup>1</sup> and C–C bond forming reactions.<sup>2–5</sup> One area of focus has been accessing formally  $\text{Ni}^{\text{IV}}$  species to test the viability of Ni as a replacement metal in reactions that invoke Pd redox couples.<sup>6</sup> These efforts have spurred important discoveries, not only in terms of the first syntheses of stable complexes bearing formally  $\text{Ni}^{\text{IV}}$  centers, but also of new applications of Ni. For example, Sanford and co-workers<sup>7</sup> reported  $(\text{Tp})\text{Ni}^{\text{IV}}(\text{aryl})(\text{CF}_3)$  ( $\text{Tp}$  = trispyrazolylborate) species that undergo formal reductive elimination to generate aryl– $\text{CF}_3$  bonds in high yields. The  $\text{Ni}^{\text{IV}}$  species  $[(\text{Me}_3\text{tacn})\text{Ni}^{\text{IV}}(\text{CH}_2\text{CMe}_2\text{o-C}_6\text{H}_4)(\text{MeCN})](\text{BF}_4)_2$  ( $\text{Me}_3\text{tacn}$  = 1,4,7-trimethyl-1,4,7-triazacyclononane) was reported by Mirica and co-workers<sup>8</sup> to generate cyclic products through C–C bond formation following illumination with blue LEDs. More recently, Nebra and co-workers<sup>9</sup> reported C–H scission and C– $\text{CF}_3$  bond forming events catalyzed by the formally  $\text{Ni}^{\text{IV}}$  species  $[(\text{py})_2\text{Ni}^{\text{IV}}\text{F}_2(\text{CF}_3)_2]$  ( $\text{py}$  = pyridine). Extending beyond the synthetic literature, Ni<sup>IV</sup> has even been recently implicated in the bioinorganic chemistry of NiFe hydrogenase.<sup>10</sup>

The electronic structures of formally  $\text{Ni}^{\text{IV}}$  species merit discussion. A key point of contention is the rift between the formal oxidation state arrived at by electron counting formalism and the physical oxidation state that better reflects the occupation of d-orbitals at the metal center. A recent computational examination of reductive elimination at the formally  $\text{Ni}^{\text{IV}}$  center in Sanford's  $(\text{Tp})\text{Ni}^{\text{IV}}(\text{aryl})(\text{CF}_3)$  by Klein and coworkers<sup>11</sup> suggests that these complexes bear physically d<sup>8</sup>  $\text{Ni}^{\text{II}}$  centers,

<sup>a</sup>Department of Chemistry and Chemical Biology, Cornell University, Baker Laboratory, 162 Sciences Drive, Ithaca, NY 14853, USA. E-mail: [kml236@cornell.edu](mailto:kml236@cornell.edu); [snm64@cornell.edu](mailto:snm64@cornell.edu)

<sup>b</sup>Department of Physics, Stanford University, Stanford, California 94305, USA

<sup>c</sup>Stanford Synchrotron Radiation Lightsource, SLAC National Accelerator Laboratory, Menlo Park, California 94025, USA

<sup>d</sup>Department of Chemistry, University of Michigan, Ann Arbor, Michigan 48109, USA

<sup>e</sup>Department of Chemistry, University of Illinois at Urbana-Champaign, Urbana, Illinois 61801, USA

<sup>f</sup>Department of Chemistry, Lehigh University, Bethlehem, Pennsylvania 18015, USA

<sup>g</sup>Department of Chemistry and Biochemistry, Baylor University, Waco, Texas 76798, USA

<sup>h</sup>Laboratoire Hétérochimie Fondamentale et Appliquée (LHFA), Université Paul Sabatier, CNRS, 118 Route de Narbonne, 31062 Toulouse, France

<sup>†</sup> Electronic supplementary information (ESI) available: ORCA inputs, input coordinates for calculations, experimental and calculated Ni K-edge XAS, experimental Ni  $\text{L}_{2,3}$ -edge XAS and desaturation, molecular orbital plots, correlation of Cu d-vacancy to 1s binding energy. See DOI: <https://doi.org/10.1039/d3sc02001k>

<sup>‡</sup> Current address: Department of Chemistry, Wayne State University, 5101 Cass Avenue, Detroit, MI.



and that this electron count persists along the entire reaction coordinate. This claim echoes recent investigations of the electronic structures of formally Cu<sup>III</sup> complexes that contends that such species do not have d<sup>8</sup> electronic configurations, no matter the coordination environment.<sup>12–15</sup> Rather, these species have electronic structures in which their frontier molecular orbitals—the conventional “ligand field”—are partially or completely inverted: their parentage features greater contributions from the ligand orbitals than the metal d-orbitals.

Ligand field inversion implies that electron hole character is localized to the ligand as opposed to the metal center.<sup>12,16</sup> In the case of Cu, this perspective has been used to rationalize the reactivity of [CuF]<sup>2+</sup> complexes in C–H fluorination,<sup>17</sup> and it has been offered as an explanation for why dipyrin complexes bearing formally Cu<sup>III</sup>–imido centers present electronic structures and reactivities more consistent with complexes bearing Cu<sup>I</sup>–nitrene centers.<sup>13</sup> Analogous electronic structure arguments have been leveled to explain the reactivity of formally Cu<sup>II</sup>–amido complexes in H-atom transfer and C–C bond formation.<sup>18</sup> Some of us have credited ligand field inversion as enabling C–C bond formation from formally Cu<sup>III</sup> centers by rendering ligands electron deficient and thus able to proceed through transition states consistent with intramolecular nucleophilic attack and intramolecular radical coupling.<sup>19</sup> In the case of Ni<sup>IV</sup> centers, localization of hole character to ligands appears evident in the case of *tert*-butylbenzene adducts of TpNi—in the case of the formally Ni<sup>IV</sup> complex, the coordinated alkyl is sufficiently electrophilic to be attacked by acetate to form a C–O bond.<sup>20</sup> In analogous Ni<sup>III</sup> species, this reactivity is not observed.

The functional implications of reassigning holes from the metal to its ligand in Ni complexes extend to materials science. In the early 1990s, studies revealed that Li doping of NiO semiconductors produced materials with electron holes localized on the O sites as opposed to the metal centers.<sup>21</sup> Recent studies on Ni-containing Li-rich layered oxides further probed the involvement of O redox in NiO moieties using resonant inelastic X-ray scattering (RIXS) to reveal significant oxygen hole character produced during charging of the material.<sup>22</sup> Additionally, investigation of Ni deficient NiO films showed that Ni vacancies cause ligand holes (Ni d<sup>8</sup>L state) to be formed near the Fermi level, significantly enhancing the electrical conduction in NiO.<sup>23</sup> Other studies have shown that stabilizing Ni in unconventional formal oxidation states can impart previously unattainable superconductivity in lattice nickelates.<sup>24</sup> These insights fall in line with the implication of O-localized holes as vital electronic characteristics of cuprate superconductors.<sup>25</sup>

Redox neutrality and ligand field inversion in reductive elimination by formally Ni<sup>IV</sup> species has been proposed on the basis of computational results.<sup>11</sup> We now supply experimental support for these electronic structure hypotheses using L<sub>2,3</sub>-edge XAS in concert with calibrated electronic structure calculations. Our assessment of the physical oxidation states of formally Ni<sup>IV</sup> species leverages sum-rule analysis of electric-dipole allowed Ni 2p → 3d XAS transitions.<sup>26–28</sup> In short, we show that the total integrated L<sub>2,3</sub>-edge intensity scales proportionally with Ni 3d character in acceptor orbitals using

[Ni(mnt)<sub>2</sub>]<sup>2–</sup> (mnt = maleonitriledithiolate) and [NiCl<sub>4</sub>]<sup>2–</sup> as calibrants. We extend our discussion with an experimentally-calibrated, multi-approach computational analysis of the NiF<sub>6</sub><sup>2–</sup> ion to evaluate the extent to which Ni can be pushed to a limiting d<sup>6</sup> electron count by highly electronegative fluoride ligands. We ultimately show that none of the formally Ni<sup>IV</sup> species approach the d<sup>6</sup> limit, but rather are better described as having physical d<sup>8</sup> Ni<sup>II</sup> centers.

## Results and discussion

### Count vs. configuration

In advance of the following discussion, it is worth differentiating a few key concepts concerning physical manifestations of “oxidation state”. Of primary importance is distinguishing d-count from d-configuration. The former concerns the electron density assigned to a transition metal on the basis of partitioning electrons between the metal and its ligands. Variable degrees of covalent admixture between metal d-orbitals and ligand orbitals will lead to variations in d-count, and these d-counts will be fractional. This concept, whose physical relevance was made manifest by Owen and Griffith's observation of Ir–Cl covalency in IrCl<sub>6</sub><sup>2–</sup>,<sup>29</sup> formed a basis for Jørgensen to make nuanced oxidation state assignments.<sup>16,30</sup> He argued that if hole character on the ligands in IrCl<sub>6</sub><sup>2–</sup> exceeded that on Ir, an Ir<sup>III</sup> assignment was more appropriate than Ir<sup>IV</sup>. However, experimental quantification of Cl hyperfine coupling revealed greater hole character on Ir. Thus, Jørgensen concluded a d-count of 5 and therefore an Ir<sup>IV</sup> assignment for this ion. Germane to the current topic of Ni<sup>IV</sup>, a d-count of 6 implies a quadruply oxidized Ni center—physical Ni<sup>IV</sup>. Species presenting a higher d-count would be assigned as bearing more reduced Ni centers. The hole character is attributed to the ligands, and this has consequences for reactivity (*vide infra*).

Computational methods enable a means to extract d-counts *via* electron partitioning schemes, *i.e.* population analyses. This partitioning is highly method dependent and, depending on the scheme, yields different values.<sup>31,32</sup> A more qualitative perspective is that some population analyses favor more ionic descriptions of bonding, whereas others provide more covalent descriptions. Consequently, it is important to calibrate these methods to physical observables. In the present case, sum-rule L<sub>2,3</sub>-edge XAS analysis furnishes a of quantification of d-count—this value is directly observable. The absorptivity of L<sub>2,3</sub>-edge main-lines is a reflection of the dipole-allowed nature of 2p → nd excitations. Dilution of this nd character by ligand admixture diminishes this absorptivity, and thus the integrated area of the L<sub>2,3</sub>-edge main lines directly reflects the amount of nd character in acceptor MOs, thus affording a measure of d-count.<sup>14,26–28,33</sup>

The d-configuration, on the other hand, is an integer count of valence electrons that affords a means to interpret experimental data (*e.g.* optical spectroscopy and magnetism) while remaining ambiguous concerning the nature of the electrons/holes. Although d-configurations are highly useful and frequently align with formal oxidation state assignments, problems arise through overinterpretation. To illustrate this point, we recall the visible spectrum of [NiF<sub>6</sub>]<sup>2–</sup>, which was

interpreted in 1969 by Allen and Warren<sup>34</sup> using a crystal-field multiplet approach. This approach succeeds when considering 4 valence holes bearing some d-parentage. However, a reasonable fit to Tanabe–Sugano matrices is only achieved when employing a substantially diminished electron–electron repulsion integral (Racah's *B* parameter). Thus, 4 valence holes for  $[\text{NiF}_6]^{2-}$  (or any other formally  $\text{Ni}^{IV}$ -containing species) does not imply that the d-count is 6, only that the resulting ground and excited states exhibit the state symmetry of a frontier molecular orbital (MO) manifold with 4 holes bearing some degree of Ni 3d character. In fact, we will show that the d-count for this species approaches 8, implying nickel possesses an oxidation state significantly lower than +4.

Cutsail and co-workers,<sup>35</sup> in a recent rebuttal of our study of formally  $\text{Cu}^{III}$  complexes, blurs this distinction between count and configuration to arrive at “physical  $d^8 \text{ Cu}^{III}$ ” assignments for a series of organocopper complexes. They note that these species display “highly covalent [metal–ligand] bonding interactions”. The observation of pre-edge features in the Cu K-edge XAS spectra of formally  $\text{Cu}^{III}$  species was proffered as key evidence for d-vacancies and thus “ $d^8 \text{ Cu}^{III}$ ”. However, such formally  $1s \rightarrow 3d$  transitions arise principally due to the quadrupolar mechanism, and thus cannot readily be used to quantify the parentage of acceptor orbitals. So, while one can argue that indeed there are two frontier vacancies in formally  $\text{Cu}^{III}$  complexes, their partitioning between metal and ligand cannot be extracted from a K-edge spectrum. These authors claim additional support for their assignments *via* analysis of both K pre-edge energies as well as Cu K $\beta$  X-ray emission spectroscopy (XES) energies, which are ascribed to changes in Cu 1s binding energies owing to increases in Cu  $Z_{\text{eff}}$  due to progressive oxidation of the metal center. This analysis will be discussed further below.

Klein and co-workers<sup>36</sup> recently conflated the concepts of d-configuration with d-count by coining the term “quasi-d” configuration”. Using  $[\text{Cu}(\text{CF}_3)_4]^-$  as an example, Klein assigned the complex as quasi-d<sup>10</sup> by application of an intrinsic bond order and energy decomposition analyses. In Klein's formalism, the quasi-d<sup>10</sup> configuration results from the summation of the 8 non-bonding localized Cu 3d electrons (the “intrinsic configuration” *i.e.*  $d^8 \text{ Cu}^{III}$ ) and the two electrons partitioned to copper in the four occupied localized Cu–C bonding orbitals (these possess 25% Cu 3d-character accounting for two additional Cu 3d electrons). This formalism was extended to Au complexes, with “quasi” *vs.* intrinsic d<sup>10</sup> differentiated both computationally and by qualitative comparison of L<sub>3</sub>-edge XAS profiles.<sup>37</sup> Experimental quantification of d-count was not provided (an accurate d-count cannot be provided without also obtaining L<sub>2</sub>-edges). We would argue that this is unnecessarily cumbersome as the difference in spectral profile can be ascribed to differences in d-configuration. A formally  $\text{Au}^I$  compound with an “intrinsic” d<sup>10</sup>-configuration effectively lacks frontier d-orbital vacancy. However, a formally  $\text{Au}^{III}$  compound with a “quasi-d<sup>10</sup>” configuration will have frontier vacancies with some d parentage, and thus additional XAS features. Thus, analogous to the case of  $[\text{NiF}_6]^{2-}$  described above, the d<sup>8</sup> configuration state manifold applies—“quasi-d<sup>10</sup>” is a d<sup>8</sup> configuration with

a d-count approaching 10. What is ultimately important is the nature of the vacancies, which lead to a more reduced metal center and more oxidized ligands. As will be highlighted below for Ni, it is the electron-depleted ligands that are rendered reactive, not an oxidized nickel-center.

Both Cutsail *et al.* and Klein *et al.*'s arguments invoke covalency concepts. For the purposes of the present discussion, we employ the widely used definition that within a MO-framework, metal–ligand covalency is the degree of metal and ligand character comprising a particular MO; a highly covalent metal–ligand MO possesses approximately equal contributions from both metal- and ligand-based atomic orbitals. Complications arise when the terms “highly covalent” and “approximately equal” are employed. For example, with  $[\text{Cu}(\text{CF}_3)_4]^-$ , Cutsail describes the lowest unoccupied MO (LUMO) as “highly covalent”, yet on the basis of our L<sub>2,3</sub>-edge XAS data<sup>14</sup> (and calculations from several groups<sup>38,39</sup>) it contains only *ca.* 30–35% Cu 3d character. Although the LUMO is covalent in nature, it is polarized towards the ligands, resulting in a d-count of 9.3. We therefore suggest that descriptions such as “ $\text{Cu}^{III}$  with highly covalent metal–ligand bonding” are not informative – in the case of organocopper complexes such a description inherently ignores the electron deficient nature of the ligands that promotes their reactivity. We contend that if one has an accurate d-count, obtained experimentally, theoretically using accurate methods that have been rigorously calibrated to experimental results, or through knowledge of how similar compounds behave, one can estimate the charge build-up on the ligands and hence make knowledgeable predictions regarding reactivity and stability.

What remains missing from a complete treatment is a reconciliation of a physical oxidation state with atomic charge. In the following study, we report d-counts obtained by experiment. However, charges at Ni (which are subject to variation due again to the arbitrary nature of partitioning schemes) will also be governed by partial 4s and 4p occupancy. These values are not readily probed experimentally. Consequently, d-count affords an upper limit to oxidation state, and thus will not capture the charge at metal in its entirety. However, we argue that scrutinizing this quantity is sufficient, because one expects the s and p contributions to the chemically relevant frontier MOs to be small – as will be shown in detail with  $[\text{NiF}_6]^{2-}$ , s and p contributions change the metal atomic charge by less than  $-1$ . Therefore, chemical insight is not eroded by a consideration of only the d-count, and one can accept inconsistencies between oxidation state assignments and atomic charge.

## Compounds under investigation

To extend this discussion to formally high-valent Ni, X-ray spectroscopic data were obtained for the 16 Ni complexes shown in Fig. 1. Compounds **1** and **2** are covalency calibrants; compounds **3–7** are highly fluorinated  $\text{Ni}^{II}$  species, compounds **8–11** are formally  $\text{Ni}^{III}$  species, and **12–16** are formally  $\text{Ni}^{IV}$  species.

## Ni K-edge XAS

Experimental Ni K pre-edge and rising edge XAS features for species **3–7** and **11–15** are compiled in Table 1. Representative



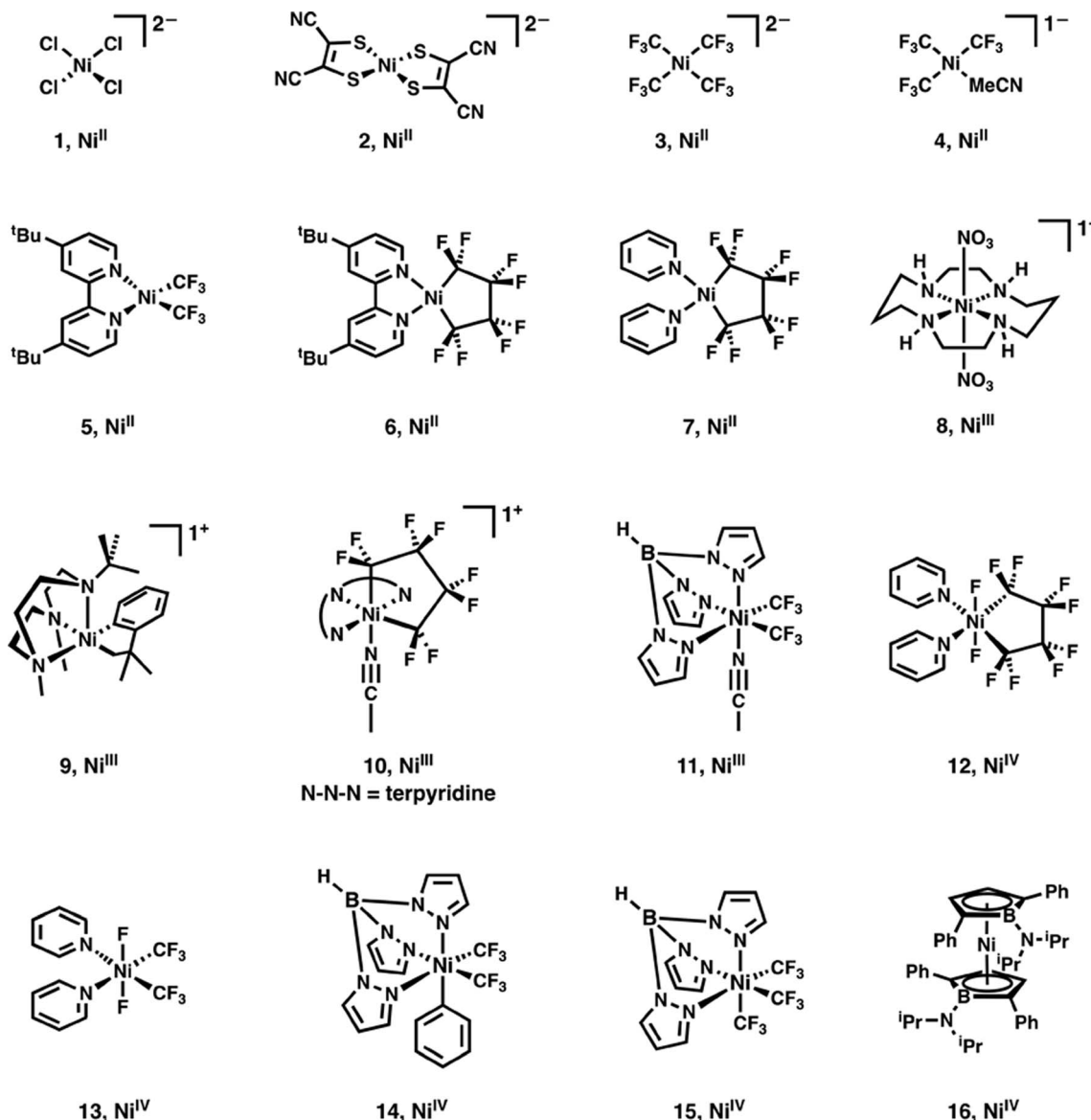


Fig. 1 Ni complexes and complex ions investigated using XAS in this study. Formal Ni oxidation states are shown below each complex.

K-edge XAS data are shown in Fig. 2a. Ni K pre-edge peak energies are plotted *vs.* formal oxidation state in Fig. 3. The data in Fig. 3 are complemented with values obtained from literature

Table 1 Tabulated Ni K-edge pre-edge and rising edge features for compounds 3–7 and 11–15

| Compound | Pre-edge energy (eV) | Edge feature 1 energy (eV) | Edge feature 2 energy (eV) |
|----------|----------------------|----------------------------|----------------------------|
| 3        | 8332.6               | 8335.2                     | —                          |
| 4        | 8332.6               | 8335.3                     | —                          |
| 5        | 8332.7               | 8334.4                     | 8336.8                     |
| 6        | 8333.0               | 8334.3                     | 8335.7                     |
| 7        | 8333.0               | 8335.4                     | —                          |
| 11       | 8333.9               | —                          | —                          |
| 12       | 8334.2               | —                          | —                          |
| 13       | 8334.0               | —                          | —                          |
| 14       | 8334.2               | —                          | —                          |
| 15       | 8334.2               | —                          | —                          |

for additional formally Ni<sup>III</sup> compounds. All species display well resolved pre-edge features between 8332.6 and 8334.2 eV. The formally Ni<sup>II</sup> species 3–7 also display one or two additional rising edge features between 8334.3 and 8336.8 eV. The pre-edge features are assigned as quadrupole-allowed excitations from Ni 1s to acceptor orbitals bearing variable amounts of Ni 3d character, and the rising edge features in the formally Ni<sup>II</sup> species are into orbitals with significant Ni d and Ni p character (Fig. S2–S9†). These assignments are supported by time-dependent DFT (TDDFT) calculations (*vide infra*). Overall, the formally Ni<sup>IV</sup> species have pre-edge features that are blue-shifted relative to formally Ni<sup>II</sup> species. As seen in Fig. 3, when only considering formally Ni<sup>II</sup> and Ni<sup>IV</sup> compounds, pre-edge peak energies exhibit a rising trend with increasing formal oxidation state. However, this does not necessarily reflect oxidation of Ni commensurate with a physical 2-electron oxidation from d<sup>8</sup> Ni<sup>II</sup> to d<sup>6</sup> Ni<sup>IV</sup>. First of all, the correlation



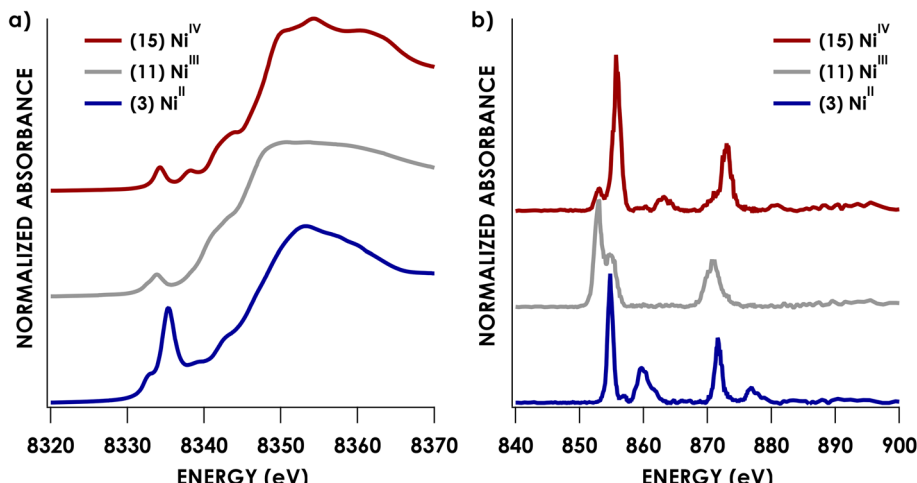


Fig. 2 Representative Ni K-edge (a) and L<sub>2,3</sub>-edge (b) XAS spectra for formally Ni<sup>II</sup>, Ni<sup>III</sup>, and Ni<sup>IV</sup> species.

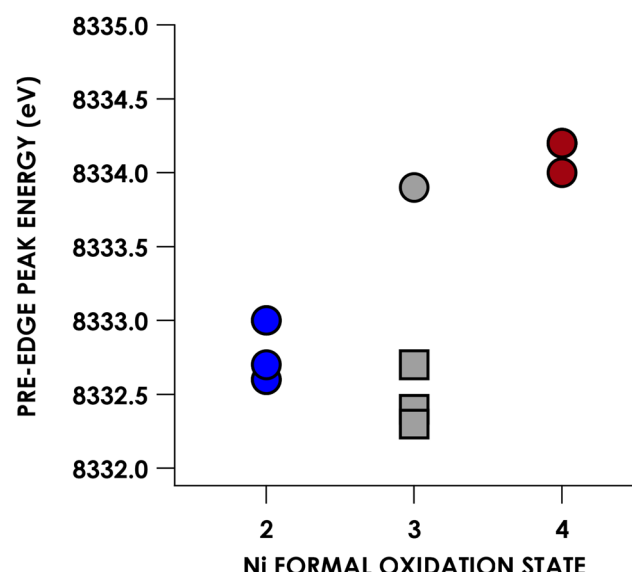


Fig. 3 Plot of Ni K-edge XAS pre-edge peak positions vs. formal Ni oxidation state for compounds 3–7 and 11–15. Gray squares correspond to formally Ni<sup>III</sup> compounds whose K pre-edge energies have been reported previously: 8332.7 eV for [Ni(<sup>II</sup>)(14-TMC)(O<sub>2</sub>)<sup>+</sup>] (12-TMC = 1,4,7,10-tetramethyl-1,4,7,10-tetraazacyclododecane),<sup>40</sup> 8332.4 eV for [Ni<sup>III</sup>(ONO<sub>2</sub>)(PyCarb<sub>2</sub>)] (PyCarb<sub>2</sub> = N,N'-(2,6-dimethylphenyl)-2,6-pyridinedicarboxamide),<sup>42</sup> and 8332.7 eV for [Ni<sup>III</sup>(NCO)(P(C<sub>6</sub>H<sub>5</sub>-SiMe<sub>3</sub>-2-S)<sub>3</sub>)]<sup>-</sup>.<sup>41</sup>

between pre-edge peak energy and formal oxidation state is disrupted by the inclusion of formally Ni<sup>III</sup> compounds including values from the literature.<sup>40–42</sup> The pre-edge peak energies of these compounds are not intermediate between those of formally Ni<sup>II</sup> and Ni<sup>IV</sup> compounds, rather, they cluster with either of the two classes of compound. This reflects the fact that pre-edge energies have contributions from both the binding energy of the metal 1s orbital as well as the ligand field strength.<sup>33,40</sup> Preferably, comparison within homologous redox series is carried out when attempting to make claims about oxidation states using K-edge XAS pre-edge features.<sup>43,44</sup> In the

present case, this is not feasible as isoleptic Ni<sup>II,III,IV</sup> series are scarce. Although rising edge energies better directly reflect charge at the metal, unambiguously assigning these energies is made difficult in the presence of large amounts of rising edge structure arising from higher-energy bound transitions (e.g. Ni(1s → 4p<sub>z</sub>) transitions), as encountered with the compounds under investigation.

Regardless, a more important point concerns 1s binding energies—these manifest with very small changes in d-count. This will be reinforced after discussion of experimentally quantified Ni d-counts—correlation of vacancy in Ni 3d with calculated Ni 1s binding energies indicates that trends in K-edge XAS energies alone should not be considered diagnostic of physical oxidation state in Ni (*vide infra*).

#### Ni L<sub>2,3</sub>-edge XAS: quantification of Ni 3d count

We and others have demonstrated that L<sub>2,3</sub>-edge XAS affords a direct means to quantify d-count.<sup>14,26–28</sup> This process is applied here for the Ni species investigated. Example Ni L<sub>2,3</sub>-edge data are shown in Fig. 2b. The remaining L<sub>2,3</sub>-edge XAS data are included in the ESI (Fig. S11–S26).<sup>†</sup> All L<sub>2,3</sub>-edge spectra were corrected for intensity saturation as described in the ESI.<sup>†</sup> The energies of L<sub>3</sub>- and L<sub>2</sub>-edge main line intensity maxima can be found in Table 2. The L<sub>3</sub>- and L<sub>2</sub>-edge main line maxima of the formally Ni<sup>IV</sup> species span over 3 eV (852.5–855.5 eV and 869.5–872.8 eV for the L<sub>3</sub> and L<sub>2</sub> respectively). Perhaps more surprisingly, the L<sub>3</sub>- and L<sub>2</sub>-edge maxima of the formally Ni<sup>II</sup> species span nearly the same range (852.7–854.8 eV and 870.9–871.7 eV for the L<sub>3</sub> and L<sub>2</sub> respectively). L<sub>2,3</sub>-edge areas found in Table 2 were obtained by fitting both the L<sub>2</sub>- and L<sub>3</sub>-edge peaks to Gaussian lineshapes and summing to obtain total areas.

(NEt<sub>4</sub>)<sub>2</sub>[NiCl<sub>4</sub>]<sup>46</sup> and {Na(benzo-15-crown-5)}<sub>2</sub>[Ni(mnt)<sub>2</sub>]<sup>48</sup> whose Ni 3d counts have been established by complementary ligand K-edge XAS measurements, were used as calibrants (Fig. 4). This calibration was then applied to obtain d-counts from experimental peak areas. Because we are probing partially occupied and/or vacant MOs, we report 3d-vacancies.

Table 2 Experimental Ni  $L_{2,3}$ -edge energies, experimental  $L_{2,3}$ -edge areas, experimental d-vacancies and calculated d-vacancies<sup>a</sup> for compounds 1–16

| Compound | Formal oxidation state | $L_3$ max. (eV) | $L_2$ max. (eV) | $L_2 + L_3$ area     | Experimental d-vacancy | Calculated d-vacancy |
|----------|------------------------|-----------------|-----------------|----------------------|------------------------|----------------------|
| 1        | 2                      | 852.7           | 871.7           | 14.7(9) <sup>b</sup> | 1.8 <sup>c</sup>       | 1.7                  |
| 2        | 2                      | 853.7           | 871.7           | 10.0(7)              | 1.2 <sup>c</sup>       | 0.9                  |
| 3        | 2                      | 854.8           | 871.7           | 9.4(7)               | 1.1(1)                 | 1.0                  |
| 4        | 2                      | 854.7           | 871.5           | 8.9(6)               | 1.1(1)                 | 1.0                  |
| 5        | 2                      | 854.1           | 870.9           | 10.8(8)              | 1.3(1)                 | 1.0                  |
| 6        | 2                      | 854.6           | 871.4           | 10.0(7)              | 1.2(1)                 | 1.1                  |
| 7        | 2                      | 854.6           | 871.4           | 12.1(8)              | 1.5(1)                 | 1.1                  |
| 8        | 3                      | 853.6           | 871.8           | 18(1)                | 2.3(1)                 | 1.8                  |
| 9        | 3                      | 852.3           | 869.7           | 12.0(8)              | 1.4(1)                 | 1.5                  |
| 10       | 3                      | 854.3           | 871.1           | 17(1)                | 2.1(2)                 | 1.6                  |
| 11       | 3                      | 853.0           | 870.7           | 15(1)                | 1.9(1)                 | 1.7                  |
| 12       | 4                      | 855.6           | 872.6           | 17(1)                | 2.1(1)                 | 1.8                  |
| 13       | 4                      | 852.9           | 871.2           | 16.7(9)              | 2.0(1)                 | 1.9                  |
| 14       | 4                      | 855.9           | 873.2           | 14(1)                | 1.8(1)                 | 1.7                  |
| 15       | 4                      | 855.7           | 873.2           | 14(1)                | 1.8(1)                 | 1.7                  |
| 16       | 4                      | 852.8           | 869.9           | 8.6 <sup>b</sup>     | 1.0(1)                 | 1.0                  |

<sup>a</sup> Calculated d-vacancies were obtained by Löwdin population analysis of RKS orbitals or UKS orbitals subjected to QRO transformation. All calculations employed the B3LYP hybrid density functional with the CP(PPP) basis set on Ni and ZORA-def2-TZVP(f) basis on all other atoms.

<sup>b</sup> Estimated saturation correction performed as 22% for 1 and 10% for 13 based on estimated tabulated transmission coefficients.<sup>45</sup>

<sup>c</sup> Experimental Ni 3d vacancy for 1 (ref. 46) and 2 (ref. 47) taken from previously reported values.

This has the added benefit of obviating the need to establish *via* calculation or otherwise the number of vacant, 3d-containing MOs. Put simply, the 3d vacancy = 10 – 3d count. To obtain these values, the experimental  $L_{2,3}$ -edge main line areas for species 3–16 are entered into the linear expression shown in Fig. 4 and then divided by 100 to obtain d-vacancies. In this manner, one finds that, *e.g.*, compound 14 is missing 1.8

electrons from a 3d<sup>10</sup> count (and thus physically lies nearer Ni<sup>II</sup> than Ni<sup>IV</sup>). *Via* this approach, one is not required to explicitly address d-configuration in order to address the discrepancy between physical and formal oxidation state. These experimental Ni 3d-vacancies are compiled in Table 2.

Two key observations may be made. The first is that formally Ni<sup>III</sup> and Ni<sup>IV</sup> complexes generally exhibit larger d-vacancies than formally Ni<sup>II</sup> compounds. A notable exception is formally Ni<sup>IV</sup> compound 16, whose d-vacancy of 1.0 places it among the values exhibited by the Ni<sup>II</sup> species. The other is that, of the compounds experimentally surveyed, no d-vacancy significantly exceeds 2—the largest value obtained is 2.3 for formally Ni<sup>III</sup>-containing compound 8.

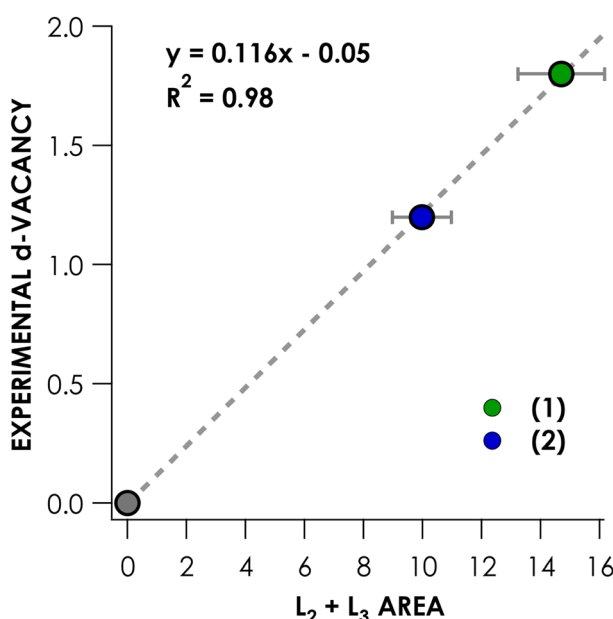


Fig. 4 Correlation between summed  $L_{2,3}$ -edge area of 1 and 2 and established Ni 3d contribution to acceptor molecular orbitals. The origin is included in the fit. Error in the slope is  $\pm 0.002$ , error in the y-intercept is  $\pm 0.02$ .

#### Influence of Ni 3d count on Ni 1s binding energy

The increase of Ni K pre-edge energies with formal Ni oxidation state, at least as presents upon comparing formally Ni<sup>II</sup> with Ni<sup>IV</sup> compounds, may appear at odds with the contention that the formally high-valent Ni species maintain physically more reduced metal centers. As discussed above, K-edge XAS and K $\beta$  XES have been used to assign a physical d<sup>8</sup> Cu<sup>III</sup> oxidation state to a series of organometallic Cu complexes by Cutsail and co-workers.<sup>35</sup> The applicability of these techniques to assign oxidation state is predicated on the metal 1s orbital binding energy being a reporter of physical oxidation state. In short, 3d orbital penetration toward the nucleus exerts some degree of shielding upon Ni 1s electrons. Thus, depopulation of 3d orbitals diminishes this shielding, resulting in shifts of the 1s orbital to a deeper binding energy. Indeed, correlation ( $R^2 = 0.94$ ) is apparent between DFT-calculated Ni 1s binding energies and pre-edge peak energies (Fig. 5a), with formally higher oxidation state complexes trending toward deeper 1s binding



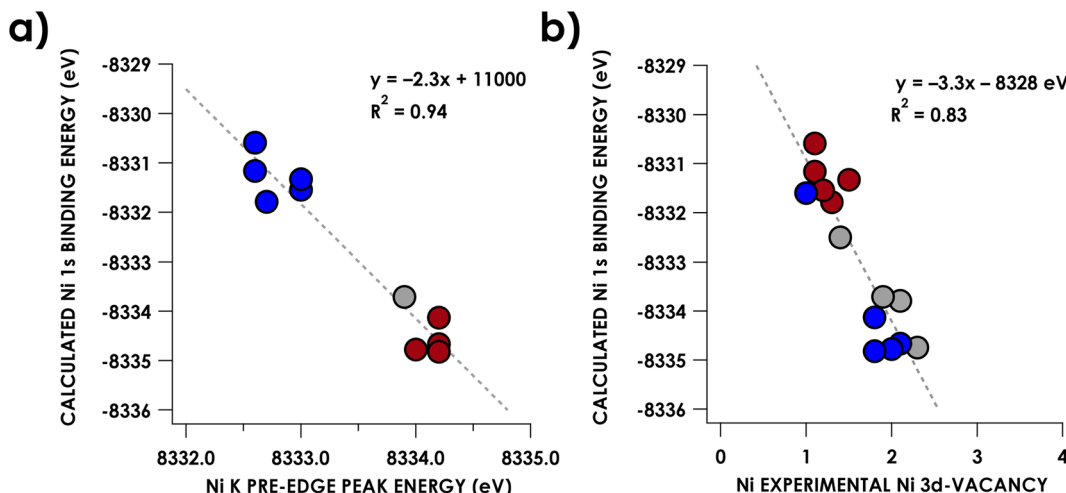


Fig. 5 (a) Plot of experimental Ni K-edge pre-edge peak energies for compounds 3–7 and 11–15 and (b) L<sub>2,3</sub>-edge sum-rule analysis derived Ni 3d vacancies vs. DFT-calculated Ni 1s orbital binding energies for compounds 3–16. Points corresponding to formally Ni<sup>II</sup> compounds are blue, Ni<sup>III</sup> in gray, and Ni<sup>IV</sup> in red.

energies. Another (weaker) correlation ( $R^2 = 0.83$ ) is encountered when plotting these calculated Ni 1s energies *vs.* the Ni 3d vacancies obtained *via* L<sub>2,3</sub>-edge sum-rule analysis (Fig. 5b). However, we note that while these shifts indeed reflect changes in valence electron population at the metal, these shifts manifest with small changes in d-population. The experimental difference in d-vacancy between the presently scrutinized complexes bearing formally Ni<sup>II</sup> centers from those bearing Ni<sup>IV</sup> centers is on the order of 1 electron. This is sufficient to manifest in *ca.* 3 eV (0.5 parts-per-thousand) changes to the calculated Ni 1s orbital binding energies – in other words, small changes in d-population result in measurably significant changes in Ni 1s binding energies. To further put this in perspective, the [Ni(mft)]<sup>2-,1-,0</sup> (mft = maleotri-fluoromethylidithiolate) series contain redox non-innocent ligands, and thus the three compounds are assigned as having an invariant physical oxidation state on nickel.<sup>49</sup> Yet they yield a change of 2.2 eV in Ni 1s binding energy over the series and corresponding measurable shifts in rising edge energy (Fig. S32†).<sup>49</sup> Regarding organocupper oxidation state assignments, this behavior is even more exaggerated for Cu where 1-electron d-vacancy changes on Cu manifest in *ca.* 7 eV (0.8 parts-per-thousand) changes in calculated 1s binding energy (Fig. S33†). This difference in changes in Ni *vs.* Cu 1s binding energies upon oxidation can plausibly be attributed to the larger  $Z_{\text{Cu}}$  *vs.*  $Z_{\text{Ni}}$ . Thus, we assert that spectroscopic signatures of 1s binding energy are insufficient to justify physical oxidation state assignments in late transition metal systems because seemingly appreciable changes to this quantity can manifest from small, non-integer changes in 3d count.

## Calculations

The finding above that, among the experimentally probed compounds, no d-vacancy significantly exceeds 2, prompts consideration of the limits to which the Ni d-manifold may be

depopulated upon oxidation of complexes/complex ions. An exhaustive collection of XAS for Ni compounds is prohibitive. To this end, we expanded our study using computational approaches, although first assuring accord with experiment for the data discussed above. We employed the B3LYP hybrid density functional, the CP(PPP) basis on Ni, and the scalar relativistically recontracted all-electron ZORA-def2-TZVP(f) basis on all other atoms. Orbital coefficients were obtained *via* Löwdin population analysis. In previous studies we found that this approach yields values that agree with experiment.

Now applied to Ni, excellent agreement ( $R^2 = 0.84$ ) is obtained when correlating DFT-calculated percent 3d-vacancies to the experimental values obtained from application of the standard curves (Fig. 6a). In a more fine-grained analysis, consideration of Ni 3d character per hole reveals agreement between experiment and theory ( $R^2 = 0.94$ ) (Fig. 6b). Orbital depictions, parentages, and Ni 3d vacancies for the formally Ni<sup>III</sup> and Ni<sup>IV</sup> species are shown in Fig. 7. Perhaps unsurprisingly, the Ni<sup>III</sup> and Ni<sup>IV</sup> species display less than 63% average Ni 3d character among their unoccupied and partially occupied MOs. However, all but one of the Ni<sup>II</sup> species also have frontier MOs with Ni d character falling well below 50% (Fig. 8), with Ni 3d orbital percentages ranging from 22% to 28%. A consensus emerges that accords with experiment: d<sup>6</sup>-count Ni<sup>IV</sup> is not encountered in any of the systems we have considered. Rather, these species have d-counts between d<sup>8</sup> and d<sup>9</sup>. The formally Ni<sup>III</sup> complexes generally exhibit d-counts similar to the Ni<sup>IV</sup> species. Additionally, the highly fluorinated Ni<sup>II</sup> (3–7) complexes are likely better described as having d-counts of d<sup>9</sup>, and thus physical Ni<sup>I</sup> centers.

## Calibrated Ni covalency calculations: application to additional reported Ni<sup>IV</sup> complexes

With the exception of 16, the formally Ni<sup>IV</sup> compounds discussed above possess highly fluorinated ligands. The agreement



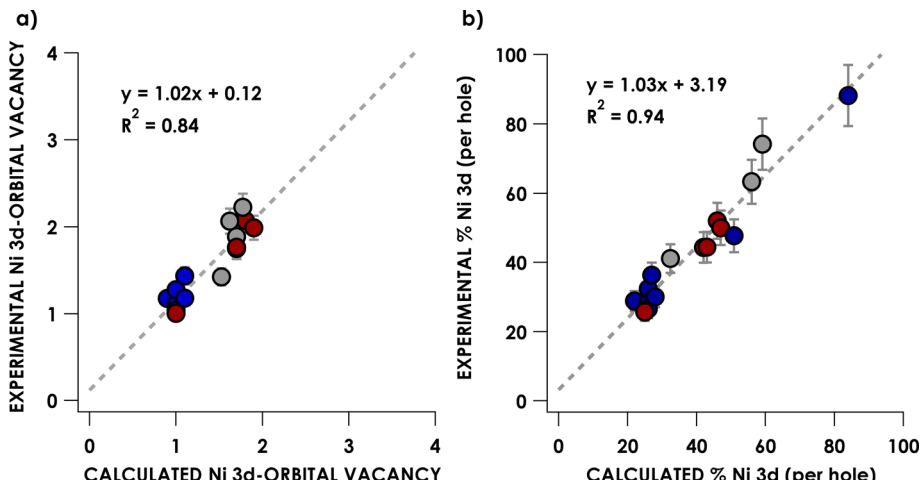


Fig. 6 Correlation between (a) experimental 3d vacancy and (b) experimental % Ni 3d character per acceptor hole with DFT-calculated values for formally Ni<sup>II</sup> (blue), Ni<sup>III</sup> (grey), and Ni<sup>IV</sup> (red) species. Errors in slope and y-intercept, respectively, are (a)  $\pm 0.06$ ,  $\pm 0.03$ ; (b)  $\pm 0.07$ ,  $\pm 0.09$ .

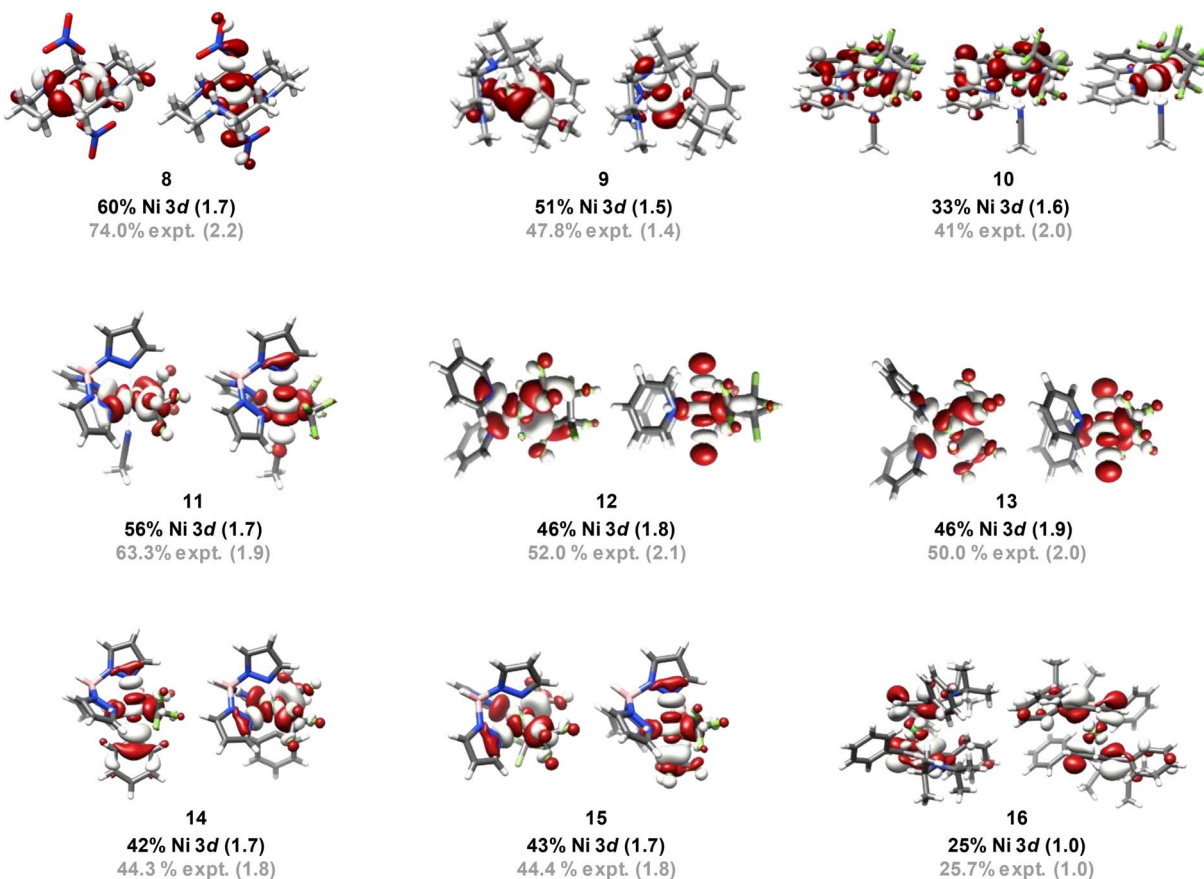


Fig. 7 Frontier unoccupied/singly occupied MOs of formally Ni<sup>III</sup> and Ni<sup>IV</sup> species. Calculated (black) and experimental (grey) averaged% Ni 3d contributions are printed below the orbitals. Corresponding 3d-vacancies are given in parentheses. Orbitals were calculated at the B3LYP/CP(PPP)/ZORA-def2-TZVP(-f) level and plotted at an isovalue of 0.03 au.

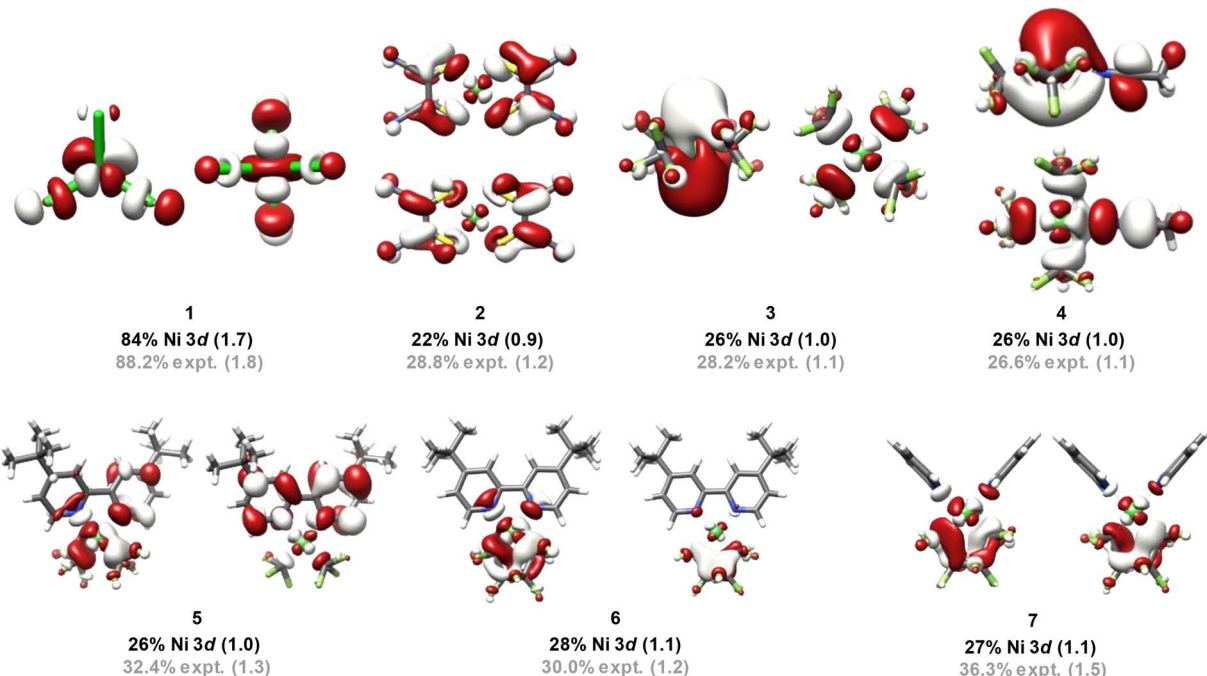


Fig. 8 Frontier unoccupied/singly occupied MOs (1–7) of formally  $\text{Ni}^{\text{II}}$  species. Calculated (black) experimental (grey) % Ni 3d contributions are given for 3–7 (for 1 and 2 only the calculated (black) and referenced experimental (gray) value are given) showing that the highly fluorinated  $\text{Ni}^{\text{II}}$  species have inverted metal vs. ligand contributions. Corresponding 3d-vacancies are given in parentheses. Orbitals were calculated at the B3LYP/CP(PPP)/ZORA-def2-TZVP(-f) level and plotted at an isovalue of 0.03 au.

between sum-rule analysis of the  $\text{L}_{2,3}$ -edge XAS and  $\text{Ni}$  3d-vacancy calculated using the aforementioned hybrid DFT protocol prompted us to consider additional complexes with a greater diversity of coordination spheres. Five additional crystallographically characterized formally  $\text{Ni}^{\text{IV}}$  compounds are shown in Fig. 9.<sup>8,50–53</sup> Unoccupied frontier MOs bearing  $\text{Ni}$  3d character are shown for these compounds in Fig. S27–S31.<sup>†</sup> Summing the  $\text{Ni}$  3d hole character over the unoccupied orbitals reveals d-counts substantially greater than  $\text{d}^6$ : they range from a  $\text{Ni}$  3d vacancy of 1.1 in **18** to a vacancy of 1.8 in **21**. These experimentally-calibrated calculations thus reveal that the complexes are better described physically having d-counts that place them in the range between  $\text{Ni}^{\text{I}}$  and  $\text{Ni}^{\text{II}}$ . Thus, highly fluorinated coordination spheres are not responsible for the large rift between the formal  $\text{Ni}^{\text{IV}}$  oxidation state and the physical d-count.

#### Electronic structure of $\text{Ni}^{\text{IV}}$ in a highly oxidizing coordination environment: $[\text{NiF}_6]^{2-}$

A particularly interesting extension of the previous computational exercise is the extreme case of  $[\text{NiF}_6]^{2-}$  (22), where  $\text{Ni}$  could be considered to be in its most oxidizing environment. In 1969, the teams of Allen and Warren<sup>34</sup> as well as Reisfeld, Asprey, and Penneman<sup>54</sup> applied Tanabe–Sugano analysis to scrutinize the electronic structure of this ion. They noted extremely low values of Racah's  $B$ -parameter, with the former team obtaining a value of  $515 \text{ cm}^{-1}$  and the latter of  $485 \text{ cm}^{-1}$  (the gas-phase atomic value is  $1238 \text{ cm}^{-1}$ ). This signifies significant delocalization of the valence electrons resulting in a substantial reduction in electron/electron repulsion. Further analysis by Allen and Warren after the manner of Jørgensen<sup>55</sup> provided an estimate of the charge at  $\text{Ni}$  of  $+1.6$ .<sup>34</sup> The d-count implied by this analysis can be no greater than 8.4, and thus the

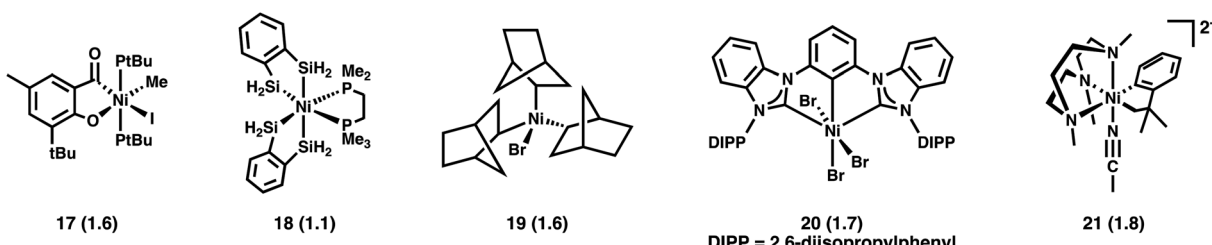


Fig. 9 Structurally characterized formally  $\text{Ni}^{\text{IV}}$  complexes investigated by experimentally-calibrated DFT calculations.  $\text{Ni}$  3d-vacancies from the calculations are given in parentheses.



physical oxidation state is more appropriately assigned as  $\text{Ni}^{\text{II}}$ , rather than  $\text{Ni}^{\text{IV}}$ .

Early semi-empirical MO calculations by Allen and co-workers<sup>56</sup> using the complete neglect of differential orbital overlap (CNDO/s) method yielded a d-count of 7.4 at Ni ( $\text{Ni}^{\text{III}}$  oxidation state) in 22; depending on the semi-empirical method used we arrive at d-counts ranging from 7.1 to 8.2. Considering the variation in the d-count based on the choice of semi-empirical method, we revisited the electronic structure of 22 using a variety of modern quantum mechanical methods, including: hybrid DFT, post-Hartree-Fock (HF), and *ab initio* valence bond (VB) methods.

The MO diagram resulting from a B3LYP calculation for 22 is presented in Fig. 10. The calculated % Ni 3d character of the vacant  $e_g$  orbitals is 57%. Employing the correlation established using the experimental spectra and plotted in Fig. 6a, this corresponds to a predicted 62% experimental Ni 3d character. This translates to a d-vacancy of 2.4 (a d-count of  $d^{7.6}$ ), or a physical oxidation state intermediate between  $\text{Ni}^{\text{II}}$  and  $\text{Ni}^{\text{III}}$ . Scrutinizing the MO diagram more thoroughly reveals that the fully occupied  $t_{2g}$  manifold (that would correspond to the canonical  $O_h$  ligand field  $t_{2g}$  orbitals) comprises only 40% calculated Ni 3d character and lies interspersed among the non-bonding F 2p lone-pair MOs. What would conventionally be considered the “ligand”  $t_{2g}$  manifold lies to deeper binding energy and contains the residual 60% Ni 3d character. Taken together, this implies that in  $\text{NiF}_6^{2-}$ , Ni 3d and F 2p are effectively isoenergetic, indicating that even with highly oxidizing

fluorine, the  $\text{Ni}^{\text{IV}}$  physical oxidation state is not achieved. This contention is reinforced through *ab initio* VB calculations that explicitly consider covalent and ionic configurations.<sup>57</sup>

The many-electron VB wavefunction ( $\Psi_{\text{VB}}$ ) results from a linear combination of Heitler–London–Slater–Pauling (HLSP) state functions ( $\Phi_i$ ) weighted by structural coefficients  $C_i$ . To limit the number of state functions, the electrons and VB orbitals ( $\varphi_k$ ) were divided into active and inactive electrons/orbitals; only those explicitly involved in bonding were considered active. Based on initial calculations at the VBSCF level,<sup>58</sup> where  $\varphi_k$  are identical in each HLSP state function, we identified four dominant VB configurations (along with their symmetry related configurations) that strongly contribute to the overall VB wavefunction (Fig. 11).<sup>59</sup> These configurations all contain Ni–F (covalent) and  $\text{Ni}^{+n}\cdots\text{F}^-$  (ionic) bonding interactions. At the VBSCF level it is already apparent that the totally ionic  $[\text{Ni}^{4+}\text{F}_6]^{2-}$  description of 22 is untenable; when included in the VBSCF calculation we find that the totally ionic HLSP state function lies 7.9 eV above the next lowest energy  $\Phi$  and does not contribute to the total VB wavefunction.

More accurate VB results can be obtained at the localized breathing orbital VB (L-BOVB) level of theory.<sup>60,61</sup> Here the  $\varphi_k$  functions are still localized on their individual atomic centers, but are allowed to optimize (breathe) for each individual HLSP state function. It has been shown that these methods give results comparable to high-level molecular orbital methods (e.g. CCSD(T) and full-CI calculations), and more accurate contributions of ionic configurations,<sup>62</sup> which we find are

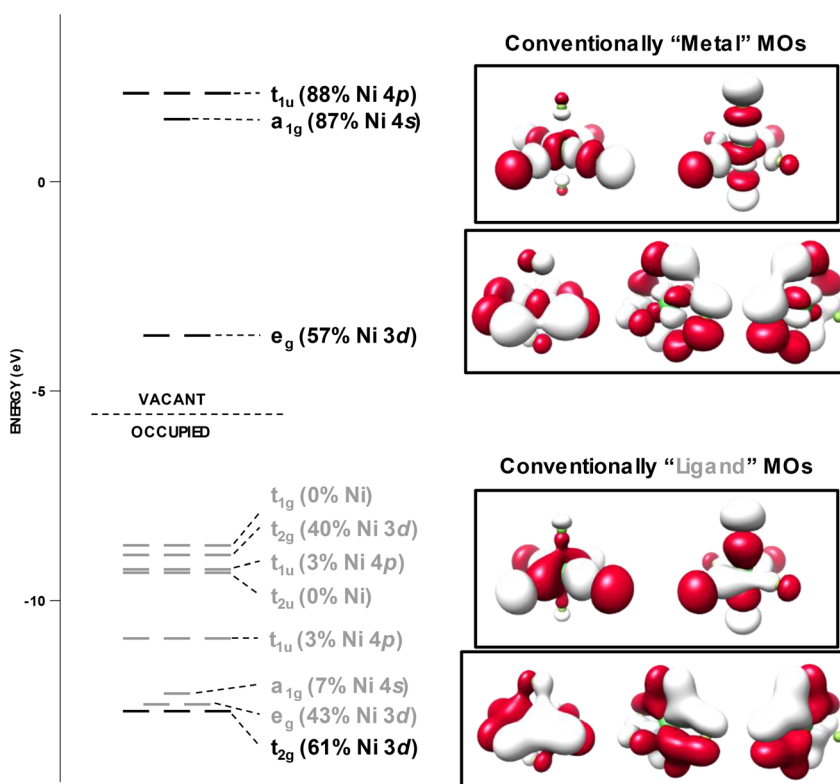


Fig. 10 Frontier MO diagram for  $\text{NiF}_6^{2-}$  calculated at the B3LYP/CP(PPP)/ZORA-def2-TZVP(-f) level. Predominantly metal-based orbitals are black, ligand-based orbitals are gray. Orbitals are plotted at an isovalue of 0.03 au.



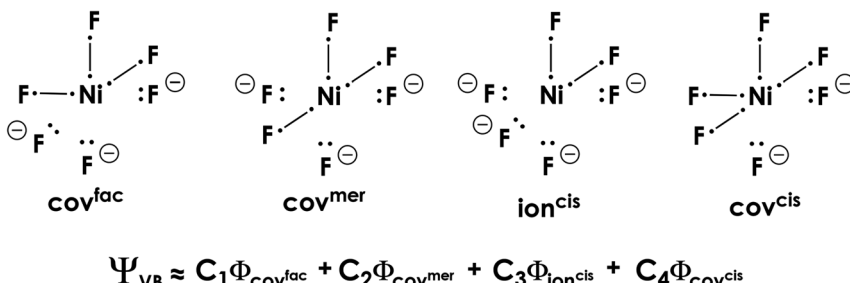


Fig. 11 Heitler–London–Slater–Pauling (HLSP) state functions of 22 that dominate the overall valence bond wavefunction. Only the active orbitals/electrons are depicted.

underweighted at the VBSCF level of theory. At the L-BOVB level we obtain a  $\Psi_{VB}$  that is predominantly  $[\text{Ni}^+ \text{F}_3 \text{F}_3^-]^{2-}$  in character (74.3%) with minor contributions by the  $[\text{Ni}^{2+} \text{F}_2 \text{F}_4^-]^{2-}$  (14.5%) and  $[\text{Ni}^0 \text{F}_4 \text{F}_2^-]^{2-}$  (11.2%) configurations (Fig. 12).

These *ab initio* VB results accord with high level hybrid-DFT and post-HF MO calculations. The L-BOVB wavefunction yields a Ni charge of  $+1.1e$ , an average F charge of  $-0.51e$  and an average Ni–F Mayer bond order of 0.47. This coincides with B3LYP/CP(PPP)/ZORA-def2-TZVP(-f) ( $\text{Ni}^{+0.90}/\text{F}^{-0.48}/\text{Ni}-\text{F}$  B.O. = 0.69), PBE0/def2-QZVPP ( $\text{Ni}^{+1.39}/\text{F}^{-0.57}/\text{Ni}-\text{F}$  B.O. = 0.61) and CCSD(T)/def2-QZVPP ( $\text{Ni}^{+1.10}/\text{F}^{-0.52}/\text{Ni}-\text{F}$  B.O. = 0.52) calculations. Lastly, these calculations all suggest that, counterintuitively, the physical  $\text{Ni}^{1+}$  center of  $[\text{NiF}_6]^{2-}$  is best described as a  $3d^8$  ion! In the VB calculations, the nickel-based valence bond orbitals involved in bonding are not pure Ni 3d orbitals, but instead have significant Ni 4s and Ni 4p character owing to orbital hybridization, thus reducing the total Ni 3d character. The molecular orbital calculations support a Ni  $d^8$  configuration

– Löwdin population analyses at both the PBE0 and CCSD(T) levels yield a  $\text{Ni} 3d^8 4s^{0.5} 4p^{0.5}$  configuration for the physically  $\text{Ni}^{1+}$  ion in 22.

To summarize, both VB and high-level MO calculations converge on an identical physical description of the formally  $\text{Ni}^{IV}$  center of 19; it is a low-valent  $3d^8 4s^1 \text{Ni}^I$  ion. This reinforces the notion that  $3d^6 \text{Ni}^{IV}$  is physically unrealistic. Such a conclusion can also be reached on the basis of

electronegativity arguments. Using Ni ionization energies,<sup>63</sup> we determine a Mulliken electronegativity<sup>64</sup> (scaled to the Pauling electronegativity scale)<sup>65</sup> for  $\text{Ni}^{4+}$  ( $\chi_{\text{Ni}^{(IV)}}$ ) of 25.1, demonstrating that  $\text{Ni}^{4+}$  will readily oxidize  $\text{F}^-$ . In fact, the electronegativities for  $\text{Ni}^{3+}$  through  $\text{Ni}^0$  ( $\chi_{\text{Ni}^{(m)}} = 17.3$ ;  $\chi_{\text{Ni}^{(n)}} = 10.3$ ;  $\chi_{\text{Ni}^{(l)}} = 5.1$ ;  $\chi_{\text{Ni}^{(0)}} = 1.8$ ) demonstrate that only  $\text{Ni}^0$  has an electronegativity that is less than fluorine (4.1) and the  $\text{Ni}^{1+}$  ion has an electronegativity comparable to fluorine. This is consistent with our above findings that the charge on nickel converges to  $\sim \text{Ni}^{1+}$  in  $(\text{NiF}_6)^{2-}$ . Taken together, we interpret this as such: outside of the gas phase, the  $\text{Ni}^{4+}$  ion is unstable and thus will be reduced in any ligand environment. If the extraordinarily electronegative hexafluoride ligand set about Ni is partially oxidized, then it should not be surprising that any other, less electronegative ligands will be oxidized as well.

### Formally $\text{Ni}^{IV}$ case studies

From the analyses above it becomes apparent that the majority of the Ni species investigated present with diminished Ni 3d character in their frontier molecular orbitals. Analogous to the Cu species we previously investigated,<sup>4</sup> these inverted or covalent electronic structures have bearing on reactivity.  $\text{Ni}^{IV}$  species are commonly invoked in 2-electron transfer reactions used to replace expensive and environmentally scarce metals such as Pd and Pt. The Sanford lab reported on the reductive elimination and C–C bond formation of a series of species with formally  $\text{Ni}^{IV}$  centers<sup>5</sup> including 14. Recently, through intrinsic bond orbital (IBO) analysis Klein and co-workers<sup>11</sup> invoked ligand field inversion to rationalize the C– $\text{CF}_3$  bond formation that occurs with 14. They further attribute reactivity to an attack of anionic  $\text{CF}_3$  on an electrophilic aryl cation, while the Ni center remains effectively  $\text{Ni}^{II}$  throughout the reaction. Our own IBO analysis of 14 based on our experimentally-validated calculations reveals a  $+0.54e$  charge for the coordinated C of the  $\text{CF}_3$  groups, while the coordinated C of the phenyl is calculated to have a  $-0.15e$  charge. This is in line with our conclusion that the Ni center in 14 is best described as physically  $\text{Ni}^{II}$ , at odds with a physical 2-electron reductive elimination. An electrostatic attraction between the positively and negatively charged carbons of the  $\text{CF}_3$  and phenyl groups drives reactivity, akin to our contention for the  $\text{Cu}(\text{alkyl})(\text{CF}_3)_3$  species we scrutinized previously.<sup>14,19</sup>

The localization of hole character to bound ligands in formally  $\text{Ni}^{IV}$  complexes enables intermolecular reactivity.

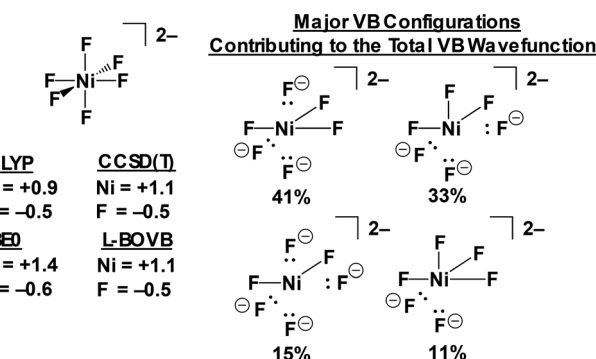
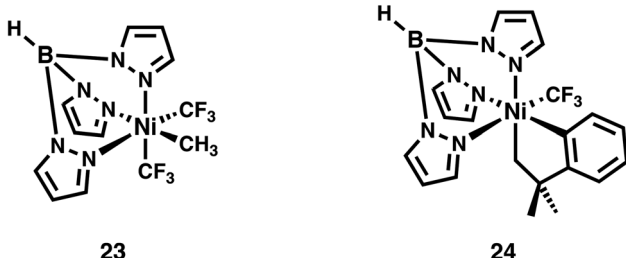


Fig. 12 Contribution of each HLSP state function to the overall valence bond wave function at the L-BOVB/Sapporo-DZVP-2012 level of theory (right). Mulliken charge on the nickel and fluorine centers at the PBE0/def2-QZVPP, CCSD(T)/def2-QZVPP and L-BOVB/Sapporo-DZVP-2012 levels of theory (bottom left).





**Fig. 13** Formally  $\text{Ni}^{\text{IV}}$  complexes whose coordinated alkyl ligands undergo C–R bond formation via attack by nucleophiles (23) or radicals (24).

Camasso and Sanford<sup>66</sup> reported that  $[(\text{Tp})\text{Ni}(\text{CH}_2\text{CMe}_2-o\text{-C}_6\text{H}_4)(\text{CF}_3)]$  (23), which has a calculated d-vacancy of 1.6, undergoes nucleophilic attack by a range of nucleophiles resulting in functionalization and detachment of the coordinated *t*-butyl methyl group (Fig. 13). Similarly, Sanford and co-workers<sup>67</sup> have provided strong evidence that  $\text{TpNi}(\text{CF}_3)_2(\text{CH}_3)$  (24), which has a similar calculated d-vacancy of 1.7, reacts with radicals ( $\text{R}'$ ) to furnish  $\text{R}-\text{CH}_3$  (Fig. 13). The calculated electronic structures for 23 and 24 follow the trend discussed above, where the metal d-count is intermediate between  $d^8$  and  $d^9$ . In both cases, there is a large degree of hole character localized to the coordinated methyl groups (Fig. 14). The reaction pathways for attack by nucleophiles (in the case of 23) or  $\text{R}'$  (in the case of 24) are thus evident. This also suggests that 24 may be

susceptible to nucleophilic attack. Similar behavior is noted for **21**, which is completely consumed upon reaction with nucleophiles, although C-X bond formation is only noted in the presence of  $\text{Cl}^-$ . Outcomes of reactions with *e.g.* acetate, azide, and other nucleophiles were not discussed in detail.<sup>8</sup>

Recently Kulka-Peschke and co-workers<sup>10</sup> proposed that oxygen tolerant [NiFe]H<sub>2</sub>ase forms a coordinatively saturated glutamate bound high-valent  $S = 0$  Ni<sup>IV</sup> state under high O<sub>2</sub> levels (Fig. 15, [NiFe]H<sub>2</sub>ase<sup>hex</sup>). This assignment was based on the lack of an EPR signal, and a good match between calculated single-determinant DFT CO/CN vibrational frequencies and experimental data. Taken at face value, one may interpret the formally high-valent Ni-center in [NiFe]H<sub>2</sub>ase<sup>hex</sup> as being an extraordinarily potent Lewis acid, which could readily promote dioxygen initiated reactive oxygen species (ROS) formation, and subsequent oxidative damage. This necessitates a coordinatively saturated Ni<sup>IV</sup> site to protect that active-site. However, our further investigation demonstrates the nickel-center of the proposed structure is itself not oxidized. A NEVPT2/CASSCF(14,13) calculation of the purported [NiFe]H<sub>2</sub>ase<sup>hex</sup> structure demonstrates that the active-site is highly multi-configurational in nature, and that the triplet state ( $S = 1$ ) rests above the singlet and quintet states (Fig. S33, Tables S1 and S2†). Furthermore, a population analysis yields a Ni d-count of 9.4, which is inconsistent with physical Ni<sup>IV</sup>. In fact, what becomes oxidized are the thiolate ligands bound to the Ni center, not the Ni or Fe centers themselves. It is the ligand environment that affords redox buffering, emphasizing the importance of coordination by biological ligands with high charge plasticity.

## Small Ni 3d vacancies in formally Ni<sup>II</sup> complexes

The disparity between formal and physical oxidation states is not unique to the unusually high valent Ni complexes, but also occurs in the formally  $\text{Ni}^{II}$  systems 2–7. As with the  $\text{Ni}^{IV}$  systems,

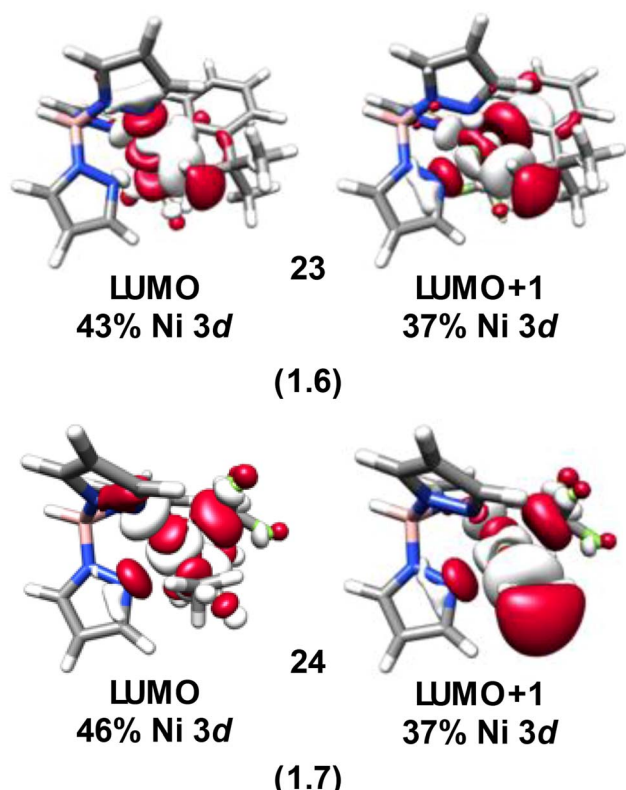


**Fig. 14** LUMO and LUMO+1 for 23 and 24 calculated at the B3LYP/CP(PPP)/ZORA-def2-TZVP(-f) level. Parenthetical values correspond to 3d-vacancies based on these orbitals. Orbitals are plotted at an isovalue of 0.03.

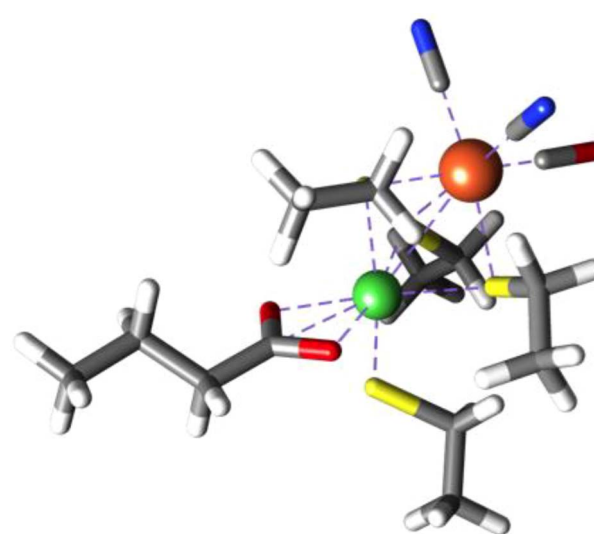


**Fig. 15** Computationally proposed structure of the active site of O<sub>2</sub>-oxidized *H. thermoluteolus* NiFe hydrogenase. Coordinates obtained from ref. 10.

fluorinated ligands are not necessary for this unconventional electronic structure, as the S-coordinated  $\text{Ni}(\text{mnt})_2$  complex 2 is also best described with a  $d^9$  count and bears no fluorinated ligands. The high covalency of these  $\text{Ni}^{II}$  systems and distribution of hole character into the ligands could have critical implications in materials science as the  $\text{NiO}$  moieties in those materials do not typically incorporate high valent  $\text{Ni}$  species, but rather  $\text{Ni}^{II}$  species that are frequently supported by O-donors.

### Implications for ligand design

Highly oxidized metal centers are a common synthetic target because of the expectation that they will exhibit enhanced reactivity. A coordination chemist may approach this using a highly anionic ligand scaffold—*e.g.* the tetraanionic tetraamidate macrocyclic ligand (TAML) scaffold or tribasic corrole ligands. Alternatively, organometallic chemists may favor ligands with a propensity for covalent bonding, *e.g.* phosphines or  $\sigma$ -alkyl donors. Regardless of the approach, the outcome is the same—successful generation of these highly oxidized species are only achieved using ligands that can surrender significant electron density to the highly electronegative metal center, not merely stabilize a high metal oxidation state through electrostatic interactions. In either case, electron deficiency manifests in the ligands, which provide loci for reactivity.

### Conclusion

The complexes discussed above showcase the generality of low  $d^n$  counts in formally  $\text{Ni}^{IV}$  centers. Furthermore, it is evident that even species with commonly observed oxidation states, such as  $\text{Ni}^{II}$ , can display similar discrepancies between their  $d^n$  counts and values implied by their formal oxidation state. The consensus picture emerges that the  $d$ -count for  $\text{Ni}$  centers in coordination and organometallic complexes remains between  $d^8$  and  $d^9$ . This accords with a proposal by Wolczanski<sup>68</sup> that the charge at  $\text{Ni}$  centers remains within 0.5e of +1.3. Additionally, we have reinforced that high metal oxidation states do not necessarily correlate to reactivity, as revealed by our discussions of the influence of electrostatic interactions of substituents, spin state and spin density on the reactivity of these species.

The use of  $\text{Ni}$  species as starting points for catalytic transformations such as C–C bond formation, C–H activation and C–H amination could enable replacement of expensive third-row transition metals in numerous catalytically relevant cycles. Furthermore, harnessing ligand oxidation in  $\text{Ni}$  containing thin films or semiconductors would allow application of this work to materials and battery chemistry resulting in more efficient substrates and transformations. We argue that analysis of all these transformations and electronic properties can be facilitated through understanding the localization of electrons, charge and radical character in the species of interest. Combined, the present work represents our continued effort to establish connections between more physically grounded oxidation states and observed reactivity that will influence further efforts in catalyst design, and materials science.

### Data availability

Data can be requested by emailing the corresponding authors.

### Author contributions

SNM, JS, and KML conceptualized the study, administered the project, collected and interpreted data, carried out calculations, and co-wrote the original draft of the manuscript. IMD synthesized compounds, collected and interpreted data, carried out calculations, and co-wrote the original draft of the manuscript. CJT and DN contributed methodology, and to both data collection and analysis. JRB, EC, DPG, C-HH, MDK, NN, LLY, and SY synthesized compounds. KML, JS, CDM, DAV, NN, and LMM acquired funding for the project. All listed authors reviewed and edited the manuscript.

### Conflicts of interest

There are no conflicts to declare.

### Acknowledgements

We thank Harry Gray, Roald Hoffmann, and Peter Wolczanski for valuable discussions. We acknowledge the NSF (CHE-1954515 to K. M. L., CHE-1753025 to C. D. M., CHE-2153730 to D. A. V., and CHE-2155160 to L. M. M.), the NIH (R15 GM141650 to J. S.), the Welch Foundation (AA-1846 to C. D. M.), and the Agence Nationale de la Recherche (ANR-JCJC-20-CE07-0023-Ni4Rf to N. N.) for support. XAS data were obtained at SSRL, which is supported by the U.S. Department of Energy, Office of Science, Office of Basic Energy Sciences under Contract No. DE-AC02-76SF00515. The SSRL Structural Molecular Biology Program is supported by the Department of Energy's Office of Biological and Environmental Research, and by NIH/NIGMS (including P30GM133894). The work at SSRL was also supported by the U.S. Department of Energy Office of Basic Energy Sciences proposal no. 100487.

### References

- 1 N. A. Harry, S. Saranya, S. M. Ujwaldev and G. Anilkumar, *Catal. Sci. Technol.*, 2019, **9**, 1726–1743.
- 2 J. B. Sweeney, A. K. Ball and L. J. Smith, *Chem.-Eur. J.*, 2018, **24**, 7354–7357.
- 3 V. P. Ananikov, *ACS Catal.*, 2015, **5**, 1964–1971.
- 4 S. Ge and J. F. Hartwig, *Angew. Chem., Int. Ed.*, 2012, **51**, 12837–12841.
- 5 S. Z. Tasker, E. A. Standley and T. F. Jamison, *Nature*, 2014, **509**, 299–309.
- 6 L. M. Mirica, S. M. Smith and L. Griego, in *Nickel Catalysis in Organic Synthesis*, John Wiley & Sons, Ltd, 2020, pp. 223–248.
- 7 J. R. Bour, N. M. Camasso and M. S. Sanford, *J. Am. Chem. Soc.*, 2015, **137**, 8034–8037.
- 8 M. B. Watson, N. P. Rath and L. M. Mirica, *J. Am. Chem. Soc.*, 2017, **139**, 35–38.

9 F. D'Accriscio, P. Borja, N. Saffon-Merceron, M. Fustier-Boutignon, N. Mézailles and N. Nebra, *Angew. Chem., Int. Ed.*, 2017, **56**, 12898–12902.

10 C. J. Kulka-Peschke, A.-C. Schulz, C. Lorent, Y. Rippers, S. Wahlefeld, J. Preissler, C. Schulz, C. Wiemann, C. C. M. Bernitzky, C. Karafoulidi-Retsou, S. L. D. Wrathall, B. Procacci, H. Matsuura, G. M. Greetham, C. Teutloff, L. Lauterbach, Y. Higuchi, M. Ishii, N. T. Hunt, O. Lenz, I. Zebger and M. Horch, *J. Am. Chem. Soc.*, 2022, **144**, 17022–17032.

11 J. S. Steen, G. Knizia and J. E. M. N. Klein, *Angew. Chem., Int. Ed.*, 2019, **58**, 13133–13139.

12 R. Hoffmann, S. Alvarez, C. Mealli, A. Falceto, T. J. Cahill, T. Zeng and G. Manca, *Chem. Rev.*, 2016, **116**, 8173–8192.

13 K. M. Carsch, I. M. DiMucci, D. A. Iovan, A. Li, S.-L. Zheng, C. J. Titus, S. J. Lee, K. D. Irwin, D. Nordlund, K. M. Lancaster and T. A. Betley, *Science*, 2019, **365**, 1138–1143.

14 I. M. DiMucci, J. T. Lukens, S. Chatterjee, K. M. Carsch, C. J. Titus, S. J. Lee, D. Nordlund, T. A. Betley, S. N. MacMillan and K. M. Lancaster, *J. Am. Chem. Soc.*, 2019, **141**, 18508–18520.

15 R. C. Walroth, J. T. Lukens, S. N. MacMillan, K. D. Finkelstein and K. M. Lancaster, *J. Am. Chem. Soc.*, 2016, **138**, 1922–1931.

16 C. K. Jørgensen, *Coord. Chem. Rev.*, 1966, **1**, 164–178.

17 J. K. Bower, A. D. Cypcar, B. Henriquez, S. C. E. Stieber and S. Zhang, *J. Am. Chem. Soc.*, 2020, **142**, 8514–8521.

18 N. P. Mankad, W. E. Antholine, R. K. Szilagyi and J. C. Peters, *J. Am. Chem. Soc.*, 2009, **131**, 3878–3880.

19 J. Shearer, D. Vasiliauskas and K. M. Lancaster, *Chem. Commun.*, 2022, **59**, 98–101.

20 C. C. Roberts, N. M. Camasso, E. G. Bowes and M. S. Sanford, *Angew. Chem., Int. Ed.*, 2019, **58**, 9104–9108.

21 M. A. van Veenendaal and G. A. Sawatzky, *Phys. Rev. B: Condens. Matter Mater. Phys.*, 1994, **50**, 11326–11331.

22 J. Xu, M. Sun, R. Qiao, S. E. Renfrew, L. Ma, T. Wu, S. Hwang, D. Nordlund, D. Su, K. Amine, J. Lu, B. D. McCloskey, W. Yang and W. Tong, *Nat. Commun.*, 2018, **9**, 947.

23 D.-Y. Cho, S. J. Song, U. K. Kim, K. M. Kim, H.-K. Lee and C. S. Hwang, *J. Mater. Chem. C*, 2013, **1**, 4334–4338.

24 D. Li, K. Lee, B. Y. Wang, M. Osada, S. Crossley, H. R. Lee, Y. Cui, Y. Hikita and H. Y. Hwang, *Nature*, 2019, **572**, 624–627.

25 Y. Guo, J.-M. Langlois and W. A. Goddard, *Science*, 1988, **239**, 896–899.

26 H. Wang, S. Friedrich, L. Li, Z. Mao, P. Ge, M. Balasubramanian and D. S. Patil, *Phys. Chem. Chem. Phys.*, 2018, **20**, 8166–8176.

27 H. Wang, P. Ge, C. G. Riordan, S. Brooker, C. G. Woomer, T. Collins, C. A. Melendres, O. Graudejus, N. Bartlett and S. P. Cramer, *J. Phys. Chem. B*, 1998, **102**, 8343–8346.

28 S. J. George, M. D. Lowery, E. I. Solomon and S. P. Cramer, *J. Am. Chem. Soc.*, 1993, **115**, 2968–2969.

29 J. H. E. Griffiths, J. Owen and B. Bleaney, *Proc. R. Soc. London, Ser. A*, 1997, **226**, 96–111.

30 C. K. Jørgensen, *Oxidation Numbers and Oxidation States*, Springer, Berlin, Heidelberg, 1969.

31 F. Neese, *Inorg. Chim. Acta*, 2002, **337**, 181–192.

32 A. Szabo and N. S. Ostlund, *Modern Quantum Chemistry: Introduction to Advanced Electronic Structure Theory*, Dover, 1996.

33 S. N. MacMillan and K. M. Lancaster, *ACS Catal.*, 2017, **7**, 1776–1791.

34 G. C. Allen and K. D. Warren, *Inorg. Chem.*, 1969, **8**, 753–756.

35 B. L. Geoghegan, Y. Liu, S. Peredkov, S. Dechert, F. Meyer, S. DeBeer and G. E. Cutsail, *J. Am. Chem. Soc.*, 2022, **144**, 2520–2534.

36 I. F. Leach, R. W. A. Havenith and J. E. M. N. Klein, *Eur. J. Inorg. Chem.*, 2022, e202200247.

37 E. A. Trifonova, I. F. Leach, W. B. de Haas, R. W. A. Havenith, M. Tromp and J. E. M. N. Klein, *Angew. Chem., Int. Ed.*, 2023, **62**, e202215523.

38 C. Gao, G. Macetti and J. Overgaard, *Inorg. Chem.*, 2019, **58**, 2133–2139.

39 J. P. Snyder, *Angew. Chem., Int. Ed. Engl.*, 1995, **34**, 80–81.

40 J. Cho, R. Sarangi, J. Annaraj, S. Y. Kim, M. Kubo, T. Ogura, E. I. Solomon and W. Nam, *Nat. Chem.*, 2009, **1**, 568–572.

41 T.-W. Chiou, Y.-M. Tseng, T.-T. Lu, T.-C. Weng, D. Sokaras, W.-C. Ho, T.-S. Kuo, L.-Y. Jang, J.-F. Lee and W.-F. Liaw, *Chem. Sci.*, 2016, **7**, 3640–3644.

42 P. Pirovano, E. R. Farquhar, M. Swart and A. R. McDonald, *J. Am. Chem. Soc.*, 2016, **138**, 14362–14370.

43 H. Kropp, A. E. King, M. M. Khusniyarov, F. W. Heinemann, K. M. Lancaster, S. DeBeer, E. Bill and K. Meyer, *J. Am. Chem. Soc.*, 2012, **134**, 15538–15544.

44 J. F. Berry, E. Bill, E. Bothe, S. D. George, B. Mienert, F. Neese and K. Wieghardt, *Science*, 2006, **312**, 1937–1941.

45 B. L. Henke, E. M. Gullikson and J. C. Davis, *At. Data Nucl. Data Tables*, 1993, **54**, 181–342.

46 E. I. Solomon, B. Hedman, K. O. Hodgson, A. Dey and R. K. Szilagyi, *Coord. Chem. Rev.*, 2005, **249**, 97–129.

47 R. Sarangi, S. DeBeer George, D. J. Rudd, R. K. Szilagyi, X. Ribas, C. Rovira, M. Almeida, K. O. Hodgson, B. Hedman and E. I. Solomon, *J. Am. Chem. Soc.*, 2007, **129**, 2316–2326.

48 D.-L. Long, Y. Cui, J.-T. Chen, W.-D. Cheng and J.-S. Huang, *Polyhedron*, 1998, **17**, 3969–3975.

49 W. Gu, H. Wang and K. Wang, *Dalton Trans.*, 2014, **43**, 6406–6413.

50 G. E. Martinez, C. Ocampo, Y. J. Park and A. R. Fout, *J. Am. Chem. Soc.*, 2016, **138**, 4290–4293.

51 V. Dimitrov and A. Linden, *Angew. Chem., Int. Ed.*, 2003, **42**, 2631–2633.

52 S. Shimada, M. L. N. Rao and M. Tanaka, *Organometallics*, 1999, **18**, 291–293.

53 H.-F. Klein, A. Bickelhaupt, T. Jung and G. Cordier, *Organometallics*, 1994, **13**, 2557–2559.

54 M. J. Reisfeld, L. B. Asprey and R. A. Penneman, *J. Mol. Spectrosc.*, 1969, **29**, 109–119.

55 C. K. Jørgensen, in *Progress in Inorganic Chemistry*, John Wiley & Sons, Ltd, 1962, pp. 73–124.



56 G. C. Allen, D. W. Clack and M. S. Farrimond, *J. Chem. Soc. A*, 1971, 2728–2733.

57 S. S. Shaik and P. C. Hiberty, *A Chemist's Guide to Valence Bond Theory*, John Wiley & Sons, 2007.

58 J. H. Van Lenthe and G. G. Balint-Kurti, *Chem. Phys. Lett.*, 1980, **76**, 138–142.

59 Consideration of Ni and F centered lone pairs in the active space did not significantly change the overall weights of the HLSP state function to  $\Psi_{VB}$ . Furthermore, those  $\phi$  constructed in terms of two-center  $3e^-$  bonds resulted in high-energy configurations that did not contribute to  $\Psi_{VB}$ .

60 P. C. Hiberty, J. P. Flament and E. Noizet, *Chem. Phys. Lett.*, 1992, **189**, 259–265.

61 P. C. Hiberty, S. H umbel, C. P. Byrman and J. H. van Lenthe, *J. Chem. Phys.*, 1994, **101**, 5969–5976.

62 W. Wu, P. Su, S. Shaik and P. C. Hiberty, *Chem. Rev.*, 2011, **111**, 7557–7593.

63 *Atomic Spectra Database*, <https://www.nist.gov/pml/atomic-spectra-database>, accessed March 15, 2022.

64 R. S. Mulliken, *J. Chem. Phys.*, 1934, **2**, 782–793.

65 Mulliken Electronegativity, [https://chem.libretexts.org/Bookshelves/Physical\\_and\\_Theoretical\\_Chemistry\\_Textbook\\_Maps/Supplemental\\_Modules\\_\(Physical\\_and\\_Theoretical\\_Chemistry\)/Physical\\_Properties\\_of\\_Matter/Atomic\\_and\\_Molecular\\_Properties/Electronegativity/Mulliken\\_Electronegativity](https://chem.libretexts.org/Bookshelves/Physical_and_Theoretical_Chemistry_Textbook_Maps/Supplemental_Modules_(Physical_and_Theoretical_Chemistry)/Physical_Properties_of_Matter/Atomic_and_Molecular_Properties/Electronegativity/Mulliken_Electronegativity), accessed March 15, 2022.

66 N. M. Camasso and M. S. Sanford, *Science*, 2015, **347**, 1218–1220.

67 J. R. Bour, D. M. Ferguson, E. J. McClain, J. W. Kampf and M. S. Sanford, *J. Am. Chem. Soc.*, 2019, **141**, 8914–8920.

68 P. T. Wolczanski, *Organometallics*, 2017, **36**, 622–631.

